



Contents lists available at ScienceDirect

Sensors and Actuators: B. Chemical

journal homepage: www.elsevier.com/locate/snb

Glutathione-activated near-infrared II fluorescent probe for lung metastatic diagnosis and intraoperative imaging of tumor

Yonghai Wang^{a,b,1}, Guiling Zhao^{a,b,1}, Yu Liu^{a,b,c,1}, Rui Wang^{a,b},
Yanlong Xing^{a,b}, Kun Dou^{a,b,*}, Fabiao Yu^{a,b,*}

^a Key Laboratory of Haikou Trauma, Key Laboratory of Hainan Trauma and Disaster Rescue, Key Laboratory of Emergency and Trauma, Ministry of Education, The First Affiliated Hospital of Hainan Medical University, Hainan Medical University, Haikou 571199, China

^b Engineering Research Center for Hainan Bio-Smart Materials and Bio-Medical Devices, College of Emergency and Trauma, Hainan Medical University, Haikou 571199, China

^c Department of Breast Surgery, The First Affiliated Hospital of Hainan Medical University, Haikou 570102, China

ARTICLE INFO

Keywords:

Near-infrared II
Glutathione-Activated
Fluorescent probe
Intraoperative tumor imaging
Lung Metastatic Diagnosis

ABSTRACT

Accurate identification of intraoperative tumor lesions and effective treatment are crucial for improving surgical outcomes. Near-infrared (NIR) fluorescence imaging demonstrates advantages over traditional medical approaches in tumor interventions, garnering significant attention. However, clinically available imaging agents are generally limited by their "always on" characteristics, which can lead to non-specific imaging interference and "false-positive" results. In this context, we present a glutathione-activated NIR-II probe, **LJ-GSH**, designed for metastatic tumor imaging and specific imaging-guided tumor resection. **LJ-GSH** initially exhibits quenched fluorescence due to the weak electron-donating effect of the thiophenol moiety, which is recovered at 815/910 nm upon activation by the overexpressed levels of glutathione (GSH) in tumor cells and tissues, significantly enhancing the specificity of tumor imaging. This unique characteristic positions **LJ-GSH** as a reliable fluorescent sensor for monitoring GSH dynamics during physiological events. Notably, the probe's NIR-II emission feature markedly improves imaging contrast and resolution, facilitating real-time identification and imaging of lung metastatic lesions. With the aid of high-specific NIR-II imaging guidance, tumor tissues can be precisely resected, with the residual negative margin diameter reduced to approximately 0.2 mm. We envision that our tailored probe may offer an attractive option for clinical applications.

1. Introduction

Malignancies, characterized by the uncontrolled growth of cancer cells and a high risk of metastasis, present a significant threat to human life and health [1–3]. Precisely monitoring the dynamic changes in tumors allows for early diagnosis and on-site evaluation of tumor development and progression, thereby enabling personalized therapy and enhancing patient survival rates [4–6]. In recent years, clinical imaging modalities such as CT, PET, and MRI have witnessed significant advances in tumor detection and localization. However, highly sensitive preoperative and intraoperative diagnosis of tumor remains a challenge for the above imaging modalities, primarily due to their limited resolution, potential radiation exposure risks, and inability to offer timely

feedback on treatment outcomes during surgery [7,8]. As an alternative tracer technology, fluorescence imaging poses significant superiority over the above medical imaging approaches in tumor interventions, benefiting from its high sensitivity, non-invasive, and fast feedback, thus, having attracted widely interesting [9–12].

Recently, efforts have focused on designing and developing fluorescent-based agents for disease diagnosis and treatment. Compared to conventional imaging probes in the visible region, fluorescence imaging in the NIR-II region (1000–1700 nm) exhibits deeper tissue penetration and higher spatiotemporal resolution due to reduced tissue autofluorescence and photon scatter, enhancing accuracy and reliability in disease detection [13–18]. Clinically approved NIR fluorescent contrast agents, such as indocyanine green (ICG) and methylene blue

* Corresponding authors at: Key Laboratory of Haikou Trauma, Key Laboratory of Hainan Trauma and Disaster Rescue, Key Laboratory of Emergency and Trauma, Ministry of Education, The First Affiliated Hospital of Hainan Medical University, Hainan Medical University, Haikou 571199, China.

E-mail addresses: doukun@muh.edu.cn (K. Dou), yufabiao@muh.edu.cn (F. Yu).

¹ These authors contributed equally to this work.

<https://doi.org/10.1016/j.snb.2024.137005>

Received 10 September 2024; Received in revised form 5 November 2024; Accepted 24 November 2024

Available online 26 November 2024

0925-4005/© 2024 Elsevier B.V. All rights reserved, including those for text and data mining, AI training, and similar technologies.

(MB), have been utilized for tumor detection and guiding tumor treatment [19,20]. However, these imaging probes typically face the challenge of short tumor retention and quick clearance from the body. Additionally, many of the currently available clinical agents display the “always on” characteristic, where they illuminate disease sites through self-accumulation rather than being specifically activated by target molecules of interest, which leads to poor imaging contrast and compromised detection accuracy. To address the issue mentioned above, stimulus-responsive fluorescence imaging strategies that can activate signal light-up only in the presence of biomarkers or pathological environments can afford higher tumor-to-normal tissue ratios (T/N ratio) and real-time biological information, making the activatable modality a preferred choice for disease diagnosis and therapy evaluation [21–25].

To develop the activation-responsive system for tumor imaging, it is crucial to carefully select a biomarker that is associated with the tumor. Studies have shown that the rapid angiogenesis, proliferation, and metastasis of tumors are linked to the overexpression of reactive oxygen species (ROS) [26,27]. To circumvent the tumor-related oxidative stress, Glutathione (GPx4) and NADPH act synergistically to maintain a cellular redox homeostasis environment via the generation of endogenous antioxidants, represented by the reduced state of glutathione (GSH). Elevated levels of GSH are commonly found in many types of tumors, and have been considered as the key indicator for discrimination of tumor region from the normal tissue [28–32]. Moreover, mitochondria are gaining increasing attention due to their critical role as the hub of metabolic activity and their potential as targets for cancer treatment. Consequently, the development of mitochondria-targeted fluorescent probes has emerged as a significant focus of research. To date, several GSH-activatable fluorescent molecular probes have been developed for detecting endogenous GSH and for further exploration of its biological role [33–38]. Despite significant advancements in GSH sensors designed for in vivo tumor imaging and therapy intervention, challenges remain. These challenges are partly due to the limited emission wavelength (less than 700 nm), undesirable mitochondrial targeting capabilities and the inadequate sensitivity of these sensors in detecting endogenous GSH levels, which typically range within the millimolar concentration.

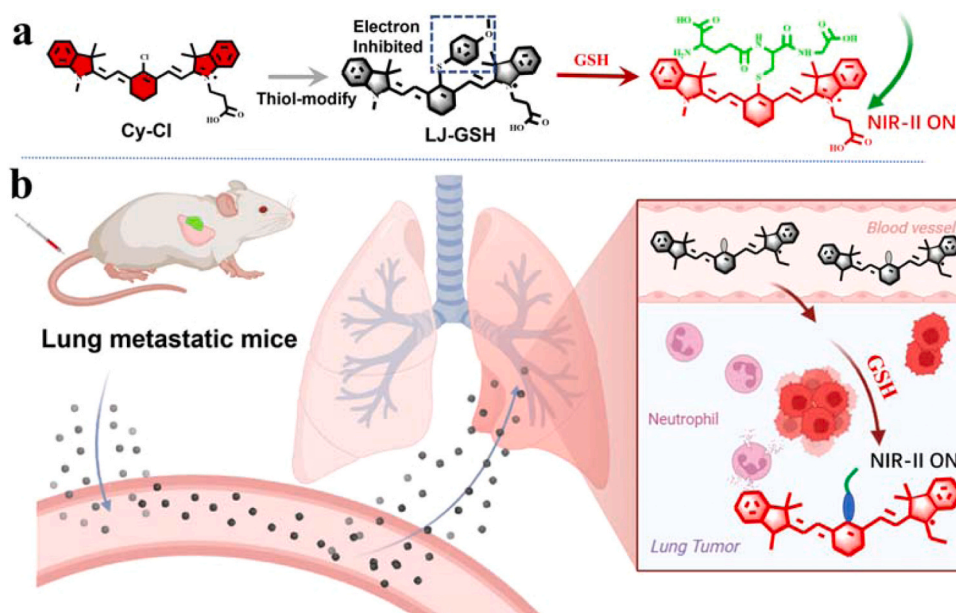
To address earlier issues mentioned, herein, we report the GSH-activatable NIR-I/II fluorescent probe for specific tumor detection and image-guided tumor resection (Scheme 1). In this study, a carboxy-modified heptamethine cyanine (Cy-7) derivative was chosen as the

fluorescence reporter due to its excellent biocompatibility and intrinsic ability to target mitochondria [39–41]. Additionally, p-Methoxy thiophenol functionality was integrated into the Cy-7 fluorophore to serve as a GSH-specific response site and fluorescence quencher, resulting in the fabrication of the NIR fluorescent sensor **LJ-GSH**. Initially, **LJ-GSH** exhibits a weak fluorescence signal due to the fluorescence quencher effect of the thiophenol site. However, upon exposure to a solution containing GSH, the GSH reacts with the probe through aromatic nucleophilic substitution, leading to the formation of a thiol skeleton with enhanced electron transfer and the subsequent emission of the bright optical signal. In vitro studies have shown that **LJ-GSH** demonstrates a suitable response sensitivity (0–10 mM GSH) and high specificity for GSH, with an emission maximum at 815/910 nm. This unique characteristic makes **LJ-GSH** a reliable fluorescent tool for discriminating tumor cells from normal ones based on GSH content discrepancy. Additionally, distinct fluctuations in GSH levels during the oxygen-glucose deprivation model process were monitored with real-time fluorescence imaging. More importantly, in combination with its NIR-II emission and GSH-specific activation characteristics, the probe **LJ-GSH** demonstrated promising capabilities for the precise localization of subcutaneous tumors and lung metastatic lesions, achieving the accurate removal of tumors with negative margins as small as 0.2 mm in diameter.

2. Materials and methods

2.1. In vivo tumor imaging and image-guided tumor resection

Four-week-old female BALB/c nude mice were purchased from Shilaikejingda Co., Ltd. (license No: SCXK 2019-0004, Hunan, China), and bred at Hainan Medical University Laboratory Animal Center. All surgical procedures and experimental protocols were approved by the Animal Care and Use Committee of Hainan Medical University (HYLL-2021-184). 50 μ L PBS containing 1×10^7 4T1 cells were transplanted around the armpit or hind legs of female nude BALB/c mice to establish the animal experiment models. When their size was about 200–300 mm³, mice were randomly assessed for imaging experiments. Firstly, to verify the feasibility of our probe in precise tumor imaging, **LJ-GSH** (100 μ L, 1 mM in physiological saline containing 1 % Tween-80 and 4 % DMSO) was intravenously injected into mice, and then, time-dependent NIR-I imaging were acquired using IVIS Lumina XR imaging system



Scheme 1. (a) Schematic illustration of probe **LJ-GSH** design and response strategy. (b) Schematic describing the mechanism of utilizing **LJ-GSH** for NIR-II imaging-guided lung metastatic lesions diagnosis.

(Excitation : 740 nm, Emission: 780–825 nm). At 24 h post-injection, tumor and other organs (liver, lung, spleen, heart, stomach, kidney) were collected for ex vivo imaging. It should be mentioned that fluorescence imaging in the NIR-II region has become the promising approach for tumor localization and intraoperative guidance of surgical navigation. In this end, **LJ-GSH**-based in vivo tumor was conducted by NIR-II imaging system. Finally, image-guided surgical resection was performed at 24 h administration of probe, and under the guidance of NIR-II imaging, the tumor was precisely resected. NIR-II images were collected using an InGaAs camera equipped with the 808 nm laser and a 900 nm long-pass filter (40 mW/cm²; exposure time, 20 ms).

2.2. In vivo lung metastasis imaging

10 days after the intravenous injection of 100 μ L 4T1-Luci tumor cells (1×10^6) into mice, **LJ-GSH** (100 nM) was intravenously injected into the mice, and fluorescence imaging in the NIR-II region was captured. Then, representative bioluminescence image was obtained to localization of the tumor position and validate the reliability of probe's fluorescence imaging. Afterward, at 24 h post-injection of **LJ-GSH** (100 nM), mice were dissected, and the ex vivo lung image observed an obvious NIR-II fluorescence signal. Finally, lung metastatic sites and normal lung tissue were further analyzed by H&E and Ki67 staining. NIR-II images were collected using an InGaAs camera equipped with the 808 nm laser and a 900 nm long-pass filter (40 mW/cm²; exposure time, 20 ms).

3. Results and discussion

3.1. Design and synthesis of GSH-responsive NIR-II probe LJ-GSH

Developing a fluorescent diagnostic probe for tumor applications, the ideal imaging agent should meet the following prerequisites: (1): NIR fluorescence emission for deep-tissue penetration and minimize auto-fluorescence; (2) tumor-related biomarker activation to enhance tumor imaging contrast (3): a highly specific response to the biomarker for increasing the accuracy in tumor diagnostics. To this end, we selected Cy derivative as the fluorescent scaffold considering its NIR emits characteristic, easy modification and favorable biocompatibility. Then, p-Methoxy-modified thiophenol, as the GSH reaction site and a fluorescence quencher, was incorporated into Cy skeleton to prepare probe **LJ-GSH**. The synthesis of the probe followed the route shown in

Scheme S1, and the compound was characterized using nuclear magnetic resonance (¹H/¹³C NMR) and high-resolution mass spectrometry (ESI-HRMS) (**Supporting information Figure S17–20**).

3.2. Spectroscopic characteristics and optical response of LJ-GSH to GSH

To demonstrate the feasibility of using **LJ-GSH** for detecting GSH in vitro, absorption and fluorescence spectrum of the probe were initially studied in PBS buffer (PBS/DMF, 9:1, v/v, 10 mM, pH 7.4, 37 °C) both in the absence and presence of GSH. As shown in **Fig. 1a&S1a**, **LJ-GSH** inherently showed a faint absorption and emission peak at 780/815 nm due to the p-Methoxy-thiophenol functionality restricted the electron transfer of the probe. Upon introducing GSH (0–10 mM) to the probe system, the enhanced absorption peak at 782 nm appeared, along with fluorescence “turn on” response at 815 nm (**Fig. 1a-b&S1b**). Furthermore, the GSH-trigger NIR-II fluorescence response at 910 nm was observed at 808 nm excitation, with the emission spectrum being board and extending into the NIR-II region (1000–1200 nm) (**Fig. 1c**). These photophysical changes were ascribed to the conversion of **LJ-GSH** into its thiol form through aromatic nucleophilic substitution, followed by enhanced intramolecular electron transfer. Then, the sensitivity and specificity of **LJ-GSH** to GSH were investigated in PBS buffer. After treating increasing levels of GSH, dose-dependent absorption/fluorescence signals were collected ($\Phi = 0.08$), and the fluorescence intensity at 815 nm was linearly proportional to GSH concentration (0.25–2.0 mM). The limit of detection for GSH was determined to be 75 μ M using the 3σ /slope method (**Fig. 1d-e**), indicating that probe endows a suitable response range and sensitivity for monitoring GSH levels dynamically (**Table S1**). Subsequent experiments on specificity and interference of **LJ-GSH** to GSH and other physiological species, such as metal ions, reactive oxygen species (H₂O₂, HClO) reactive sulfur species (Cys, Hcy, NaHS, Na₂S₄) and reactive nitrogen species (ONOO⁻, NO), were conducted. Results from **Fig. 1f&Fig. S2** suggested that minimal fluorescence response was found when other interfering targets were introduced, and only GSH led to an evident fluorescence enhancement.

It is known that a fast response rate enables real-time monitoring of dynamic processes, and kinetic studies revealed that the fluorescence maxima can be reached within 30 min (**Fig. S3a-b**). Furthermore, we confirmed that **LJ-GSH** exhibited good stability over the pH range from 4 to 9 in PBS buffer. Meanwhile, the optical signal of **LJ-GSH** after reacting with GSH within the pH verified from 6.5 to 8.0 was hardly

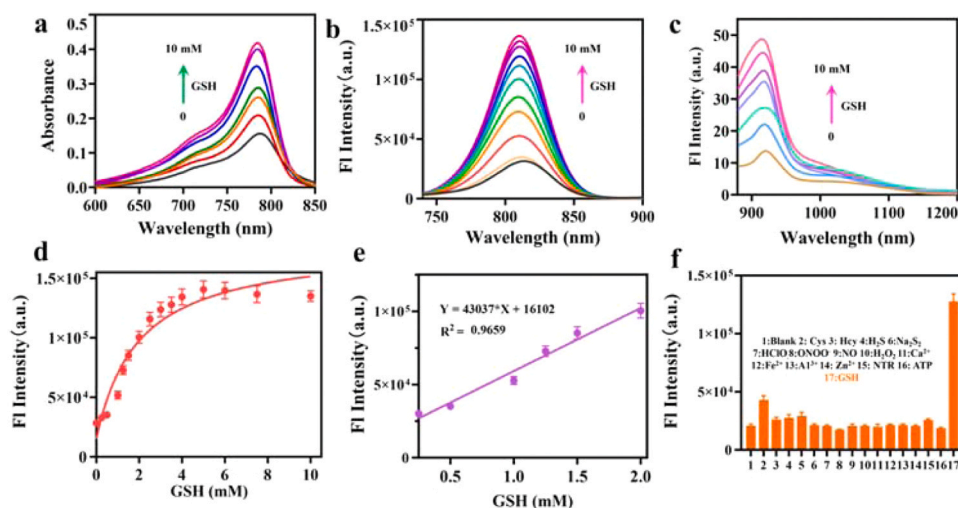


Fig. 1. (a) Absorption spectra of **LJ-GSH** (10 μ M) upon the addition of 0–10 mM GSH; (b) NIR-I, and (c) NIR-II FL spectrum of **LJ-GSH** (10 μ M) after treatment with different concentrations of GSH (0–10 mM). (d) Titration curve of **LJ-GSH** (10 μ M) to 0–10 mM GSH; (e) Linear relationship between fluorescence intensity at 815 nm and [GSH] in the range of 0.25–2.0 mM; (f) NIR-I FL response of 10 μ M **LJ-GSH** to various interfering species and GSH. $\lambda_{\text{ex}} = 808$ nm for NIR-II, and $\lambda_{\text{ex}} = 720$ nm for NIR-I.

influenced, suggesting its promise for monitoring the fluctuation in GSH levels during both physiological and pathological processes (Fig. S4a-b). Stability in the presence of serum was also evaluated owing to possible interactions in an organism, and the results depicted in fig. demonstrated that negligible effect on LJ-GSH fluorescence upon coincubation of 0–24 h (Fig. S5). Finally, both LJ-GSH and its reaction product maintained a relatively stable optical signal when exposed to continuous Xe lamp radiation for 20 min ($\text{Ex} = 720 \text{ nm}$, Fig. S6). To verify the response mechanism of the probe to GSH, a high-resolution mass spectrometry analysis of LJ-GSH in the presence of GSH was conducted. As shown in Fig. S7, an expected ion peak (m/z) at 812.3678 was identified (calculated value: 812.3688), thereby confirming the GSH-mediated nucleophilic substitution mechanism.

3.3. Applicability to live cell imaging

Encouraged by the favorable optical responsivity of LJ-GSH to GSH in PBS buffer, subsequent experiments were carried out to assess the probe's capability to monitor the fluctuations of endogenous GSH in living cells. Firstly, the 3-(4,5-dimethylthiazol-2-yl)-2,5-phenyltetrazolium bromide (MTT) assay was used to evaluate the probe's cytotoxicity. After the 4T1 cells were incubated with increasing concentration of probe (0–10 μM) for 12 h, over 80 % were alive, indicating a high compatibility of the probe (Fig. S8). Subsequently, we explored the photo-stability of LJ-GSH in cellular imaging. After 30 min incubation, cells were administrated into the confocal microscope, and the fluorescence signal of LJ-GSH in cells maintained relative stability under continuous laser radiation (633 nm) for over 5 min (Fig. S9a-b). To better understand the distribution of LJ-GSH in cells, we then performed the colocalization test by co-incubation of the probe with a commercially available fluorescent dye Mito-Tracker Green. As shown in Fig. S10, the fluorescence signal in the red channel showed significant overlap with the green channel, and Pearson's correlation coefficient was calculated as 0.93.

Inspired by the promising mitochondria-targeted capability of the probe, we investigated the real-time monitoring of dynamic fluctuations in mitochondria GSH. Upon loading cells with 10 μM of the probe for 30 min, a strong fluorescence signal in the red channel was observed, indicating that LJ-GSH could be activated by endogenous GSH (Fig. 2a-i). To validate this hypothesis, cells were pre-treated with N-methylmaleimide (NMM), a GSH inhibitor, followed by incubation with the probe, which resulted in a 3.4-fold decrease in red fluorescence compared to the control group (Fig. 2a-ii&b). Interestingly, the addition of glutathione monoethyl ester (an exogenous GSH donor) led to a

significant fluorescence increase in the red channel, demonstrating that LJ-GSH could effectively visualize GSH dynamics within cells (Fig. 2a-iii&b). It is worth noting that tumor cells exhibit higher levels of ROS to support their rapid proliferation compared to normal cells. Additionally, accumulated ROS may disrupt redox balance and cause oxidative stress. Next, we investigated whether GSH assumption caused by H_2O_2 , a typical reactive oxygen species, could be visualized with LJ-GSH (Fig. 2a-iv&b). Indeed, Treatment with exogenous H_2O_2 led to a decreased optical signal in the red channel, indicating that tumor cells may have evolved an anti-oxidative system to scavenge cellular H_2O_2 by oxidizing GSH to GSSG. Furthermore, a similar fluorescence quencher phenomenon was found in the LPS-treated group, which is known to stimulate the production of endogenous ROS (Fig. 2a-v&vi&b).

The capability of LJ-GSH to discriminate between tumor cells and normal cells is significant for tumor-associated interventions. For this purpose, several cell lines, such as, PC 12 cells, 4T1 cells, A549 cells, U87 cells, Macrophage-Raw 264.7, and cerebral vascular endothelial cell-hCMEC/D3 (normal cells) were loaded with probe for 30 min, respectively, and then imaged under otherwise the same conditions. As shown in Fig. S11a-b, the fluorescence signals in tumor cells and Raw 264.7 showed an over 2-fold enhancement than that of normal cells, suggesting much higher GSH expression in the former. This finding may be attributed to the fact that both the tumor and macrophage cells generally possess high levels of ROS. In response, these cells develop an anti-oxidative defense system, characterized by the generation of endogenous antioxidants, represented by GSH. All above results demonstrated that probe LJ-GSH was capable of monitoring and visualizing endogenous GSH generation in cells.

3.4. Investigation of GSH biological role in the oxygen-glucose deprivation/reperfusion model

Hypoxia and inadequate energy supply induced by restricted blood supply are important features of tumors. Hence, we then investigated whether LJ-GSH could visualize GSH fluctuations and further evaluate its biological role in the oxygen-glucose deprivation/reperfusion model. After establishing the time-dependent (0–120 min) oxygen-glucose deprivation processes, probe was added to cells and the GSH dynamics were monitored using confocal imaging. Compared to the un-treated group (0 min oxygen-glucose deprivation intervention), significantly decreased fluorescence signals were observed as time progressed, indicating a marked GSH consumption under oxygen-glucose deprivation (Fig. 3ai-iv&b). Interestingly, the red fluorescence signal continued to decline even after 30 min reoxygenation and perfusion with a normal

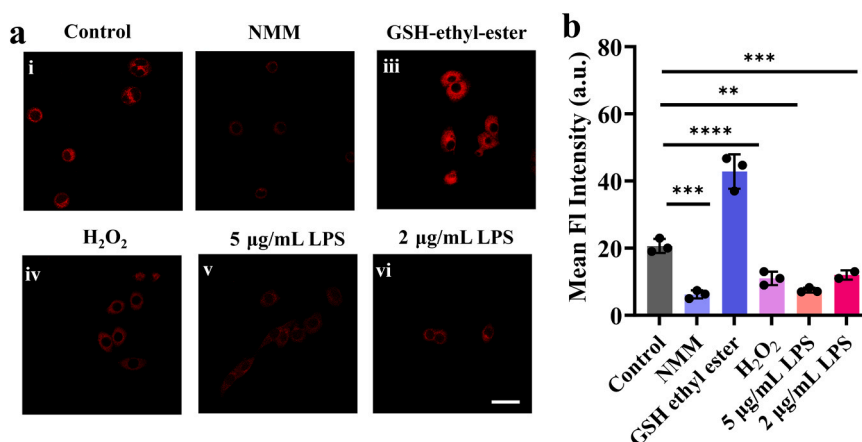


Fig. 2. (a-i) Cells were only incubated with probe (10 μM) for 30 min. (a-ii) Cells were pre-treated with 1 mM NEM for 20 min, and then cells were incubated with LJ-GSH for 30 min. (a-iii) Cells were treated with GSH-ethyl-ester (1 mM) and probe (10 μM) for 30 min. Cells were pre-incubated with H_2O_2 (0.2 mM, a-iv), 5 $\mu\text{g/mL}$ Lps (a-v), and 2.5 $\mu\text{g/mL}$ Lps (a-vi) for 2 h, and then incubated with LJ-GSH (10 μM) for 30 min. (b) Fluorescence intensity of Aa–f group cells. Data denote mean \pm s.d. ($n=3$, ** $P < 0.01$, *** $P < 0.001$, **** $P < 0.0001$). The images were recorded with 633 nm excitation and 725–800 nm collection. Scale bars: 25 μm .

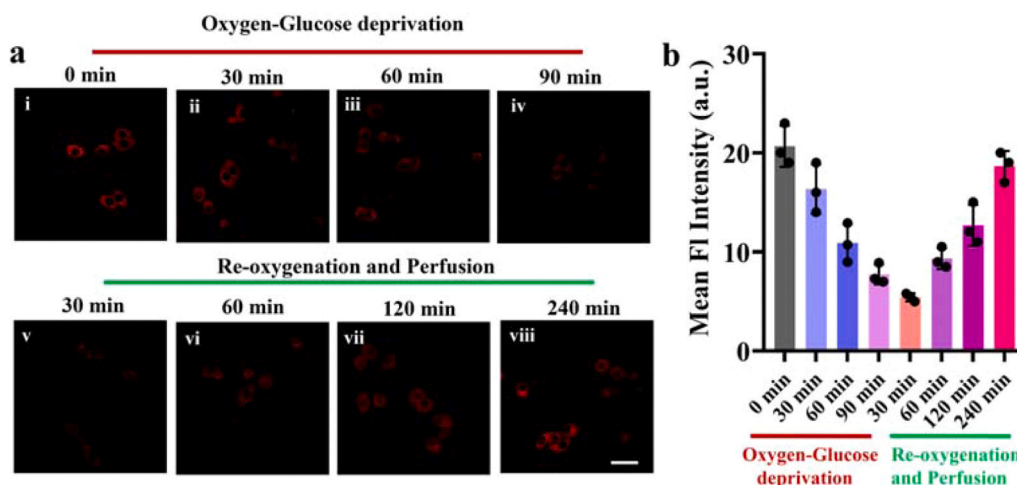


Fig. 3. (ai-iv) Time-dependent (0–90 min) real-time GSH imaging with LJ-GSH (10 μ M) in 4T1 cells under oxygen-glucose deprivation (glucose-free (0 mM: 0 G), 1 % O_2). (a-v-a-viii) After 90 min oxygen-glucose deprivation, cells were incubated with normal medium containing (25 mM glucose) and 21 % O_2 for different reperfusion time, 30 min (a-v), 60 min (a-vi), 90 min (a-vii), 120 min (a-viii), subsequent, LJ-GSH (10 μ M) were added to cells for another 30 min incubation. (b) Fluorescence intensity of ai–aviii group cells. Data denote mean \pm s.d. The images were recorded with 633 nm excitation and 725–800 nm collection. Scale bars: 25 μ m.

medium containing glucose (Fig. 3a-v&b&S12). This result may be attributed that upon restoration of oxygen-glucose supply during reperfusion, there is a sudden shift in redox balance, triggering an increase in intracellular ROS generation. Moreover, we noticed a progressive restoration of fluorescent signals in cells over time, indicating that prolonged oxygen-glucose refusion triggers a restructuring of cellular redox balance and an increase in GSH production (Fig. 3a-vi-viii&b&S12). More importantly, based on the variation of GSH as shown by the fluorescence signal, we can better understand the timing and trend of GSH dynamics, enabling timely intervention and monitoring the following therapeutic outcomes in a physiological context.

3.5. Precise delimitation of tumor and NIR-II imaging-guided intraoperative surgical resection

Encouraged by the excellent performance of LJ-GSH in cell studies, we assessed its feasibility in vivo tumor diagnosis and intraoperative guidance of tumor treatment. Initially, the biosafety of probe as the in vivo imaging contrast was evaluated. Histological analysis of major organs, including heart, liver, spleen, lung, and kidney, after 24 h post-injection of the probe revealed no significant injuries, indicating the probe's favorable compatibility (Fig. S13). Moreover, the results presented in Fig. S14 indicate that most of the probe can be metabolized from the liver within 48 h post-injection. Then, to study the tumor imaging capability of the probe, LJ-GSH was injected intravenously into 4T1 tumor mice, and time-dependent whole-body NIR fluorescence images were captured. The results illustrated in Fig. 4ai-b&S15 demonstrated a gradually increased imaging signal in tumor over time, reaching a plateau within 12–24 h post-injection. Quantitative analysis showed a nearly 2.7-fold fluorescence amplification in tumor regions compared to normal tissue (Fig. 4c). This suggests successful tumor accumulation of LJ-GSH and subsequent activation by tumor GSH. To further verify that optical imaging with longer excitation and emission wavelength has better imaging performance by reducing tissue autofluorescence and photon scattering, in vivo tumor imaging was carried out by the NIR-II imaging system. As shown in Figs. 4a-ii, 1 h after intravenous injection of the probe, the tumor tissue could be clearly distinguished from surrounding normal tissue. In the following 24 h post-injection, the fluorescence signal of LJ-GSH in tumor region continuously enhanced, and reached the maximum at 24 h PI with a T/N ratio of 5.85 ± 1.7 (Fig. 4d-e). Notably, real-time fluorescence intensity quantitation revealed that the optimal T/NT ratio for LJ-GSH in the NIR-

II imaging window was 2.2-fold higher than that obtained in the NIR-I imaging window (5.85 ± 1.7 vs 2.65 ± 0.7), verifying the superior of NIR-II imaging. According to the Rose criterion, accurate identification of image features requires a T/N ratio over 5, indicating LJ-GSH endows the potential in the precise delimitation of tumor (Fig. 4f). Finally, the ex vivo image in Fig showed that tumor tissue exhibited the strongest fluorescence signal in comparison to other organs, further verifying the probe's precise targeting and activation (Fig. 4g-i).

It should be mentioned that fluorescence imaging in the NIR-II region has become the promising approach for tumor localization and intraoperative guidance of surgical navigation, because of its inherent merits of high resolution and deep-tissue penetration. Thus, based on the favorable properties of LJ-GSH in accurate tumor localization and high-contrast imaging, fluorescence imaging-guided tumor resection was performed 24 h after administration of the probe, when the edge and outline of the tumor could be identified from the surrounding normal tissue (Fig. 4j). Under real-time image guidance, tumor tissue navigation achieved a region of interest A (ROI-A) signal-to-background ratio (SBR) of 5.77 ± 0.37 . In contrast, the SBR of the resected region (ROI-B, post-B) decreased to nearly 1, indicating complete tumor removal (Fig. 4k). To illustrate the surgical outcomes more intuitively, the optical signals of the resected tumor and the post-surgery position were analyzed according to the line marked in Fig. 4j&4l. The results indicated a prominent signal at ROI-A, while negligible signal fluctuations were observed at ROI-B. Subsequently, the resected specimen was stained with hematoxylin and eosin (H&E) for pathological diagnosis. The H&E staining analysis confirmed the reliability of our probe in tumor resection, with the residual negative margin diameter reduced to approximately 0.2 mm (Fig. 4m-n). As anticipated, tumor-bearing mice that underwent resection surgery exhibited a higher survival rate and extended survival period compared to untreated controls (Fig. 4o). Overall, the probe LJ-GSH could achieve accurate localization of tumor boundaries and provide effective assistance in tumor navigation with high-specific NIR-II imaging.

3.6. NIR-II imaging-guided lung metastatic lesions diagnosis

Metastatic dissemination resulting from incomplete tumor therapy is a major contributor to cancer-related mortality, making early diagnosis and treatment interventions are crucial to human health. Hence, metastatic lung tumor model was constructed to investigate whether the probe could identify the metastasis. 10 days after 4T1-luc cells

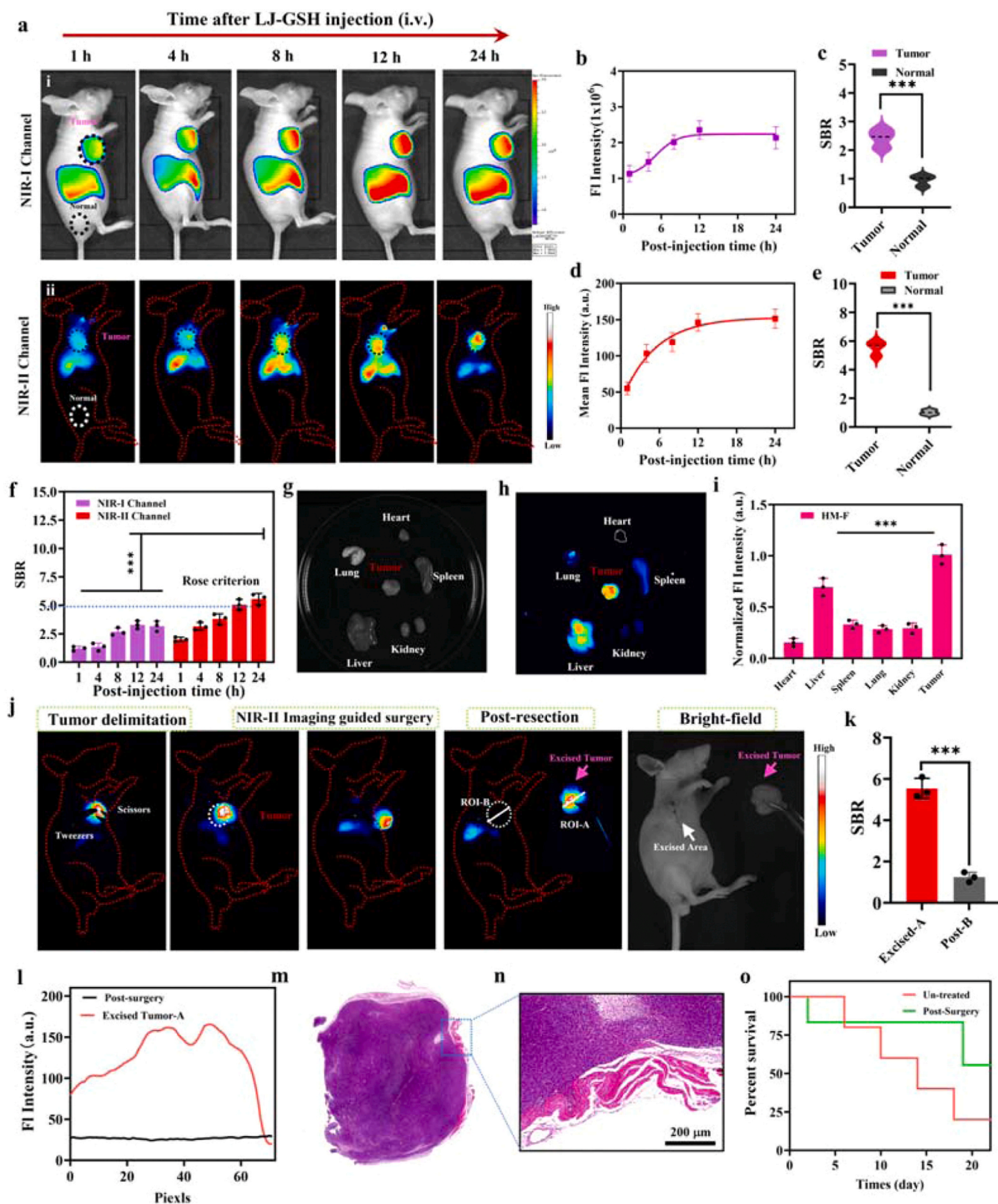


Fig. 4. (a-i) Time-dependent in vivo fluorescence imaging of GSH in tumor bearing mice at NIR-I window and (a-ii) at NIR-II window. (b) NIR-I and (d) NIR-II Fluorescence intensity in tumor region at various time points (0–24 h) after i.v. injection of LJ-GSH (100 μ L, 1 mM). (c) T/N ratios after 24 h i.v. injection of probes at NIR-I window, and (e) at NIR-II window. (f) Time-dependent T/N ratios after i.v. injection of probes. (g)-(h) representative ex vivo fluorescence images of tumor and major organs at 24 h post-injection of LJ-GSH. (i) Normalized NIR-II fluorescence intensity of the tumor and other organs in panels g. (j) NIR-II image-guided subcutaneous tumor resection. (k) SBR of the resected tumor (ROI-A) and post-surgery position (ROI-B). (l) Line profile of photon counts from j. (m)-(n) H&E staining results of excised tumor margin, Scar bar: 200 μ m. (o) Kaplan–Meier survival rate curve of five mice with or without tumor resection. NIR-I window: Ex = 745 nm, Em: 780–825 nm. NIR-II images were collected under 808 nm excitation, 900 nm long-pass filter, 40 mW/cm², and exposure time: 20 ms. n=3, Data denote mean \pm s.d. (n=3, **P<0.01, ***P<0.001, ****P<0.0001).

administration, LJ-GSH was intravenously injected into mice followed by NIR-II and bioluminescence imaging Fig. 5a. As shown in Fig.S16a, a faint fluorescence signal was observed in the thoracic cavity. We speculated that the tumor metastasis may have occurred in the lung region,

generating tumor-related GSH and triggering the activation of probe LJ-GSH. To make check, bioluminescence imaging and ex vivo lung imaging were performed. Bioluminescence signal in the thoracic cavity corresponded well with in vivo NIR-II imaging (Fig. 5b), demonstrating

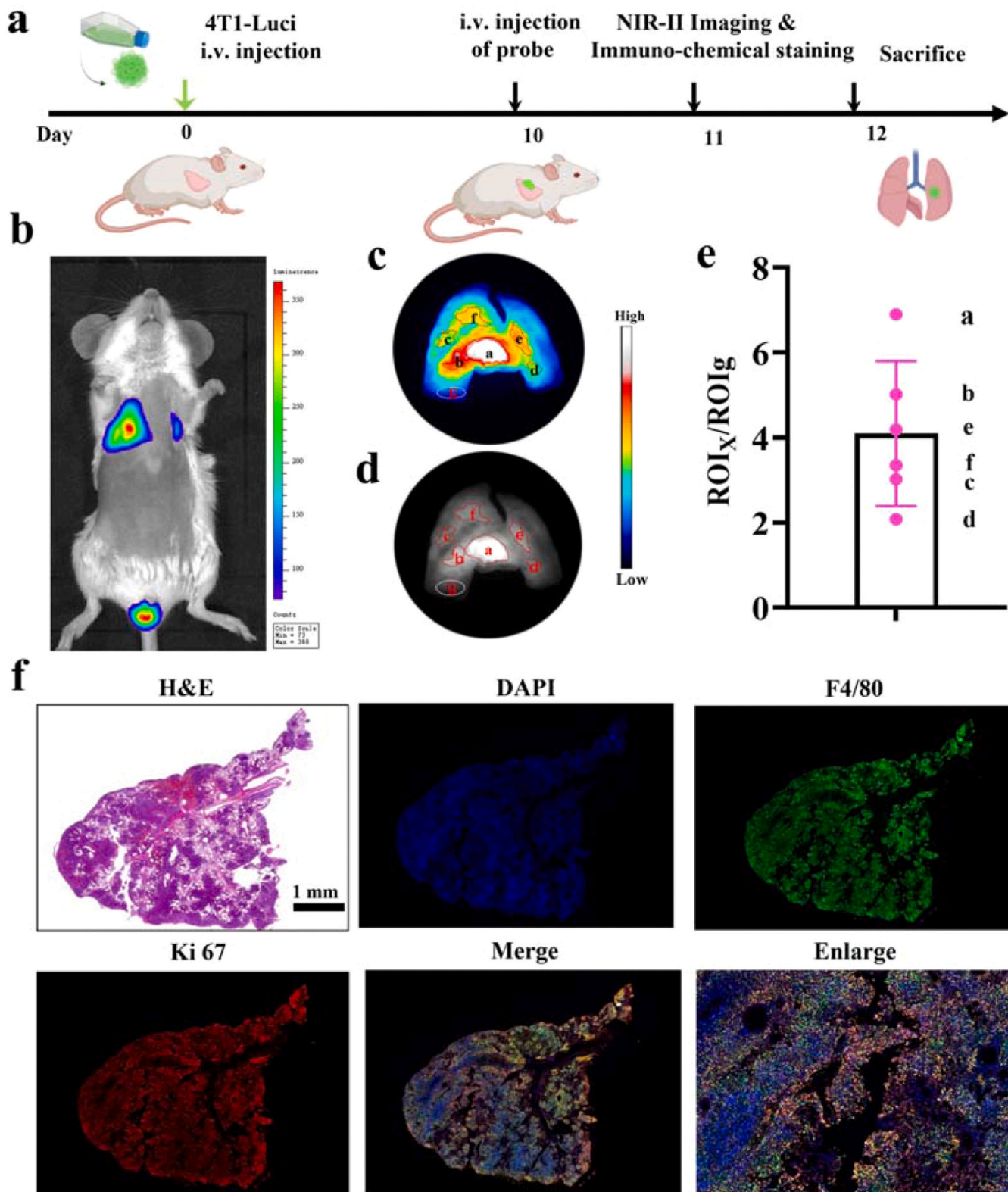


Fig. 5. (a) Schematic illustration the timeline of lung metastasis model establishment and real-time tumor imaging. (b) Representative bioluminescence image. (c)-(d) NIR-II imaging of lung tissue dissected from lung metastatic mice after 24 h post-injection of (100 nM) LJ-GSH. (e) SBR of lung metastatic tumors according to c and d (marked as a-f and control as g). (f) H&E, ki 67, and F4/80 immunofluorescence staining of the resected lung metastatic nodules (ROI-a) Scar bar: 1 mm.

the reliability of our probe in metastatic tumor applications. Meanwhile, ex vivo lung imaging revealed that pulmonary metastasis exhibited a high SBR of 7.2 (ROIa/ROIg), suggesting **LJ-GSH** has the potential for discriminating between metastatic lesions and adjacent lung tissues (Fig. 5c-e&s16b). To this end, the lung tissue of ROI-a was resected, and subsequently subjected to H&E and immunofluorescence staining tests. Based on the H&E, metastasis-related ki67 and F4/80 imaging results, **LJ-GSH** could effectively identify and navigate metastatic lesions under high-specific NIR-II imaging guidance (Fig. 5f).

4. Conclusion

In summary, based on cyanine fluorophore, we reported the GSH-activated NIR-I/II fluorescent probe, **LJ-GSH**, for specific lung metastasis imaging and fluorescence-guided surgical navigations. The probe initially exhibits fluorescence quenching due to the inhibited electron transfer process from p-Methoxy thiophenol functionality to cyanine moiety. Upon interaction with GSH, **LJ-GSH** converts to its thiol form through GSH-mediate nucleophilic substitution, releasing NIR-I/II emission (815/910 nm) with recovery of electron transfer. In vitro analysis tests have shown probe displays high specificity and suitable sensitivity to GSH, making **LJ-GSH** a promising tool for imaging GSH dynamics in cells. Benefiting from the high resolution and high-specific NIR-II fluorescence imaging from **LJ-GSH**, subcutaneous and metastasis breast lesions are clearly distinguished from surrounding normal tissue, with negative margins as small as 0.25 mm in diameter. We expected that **LJ-GSH** could offer a valuable approach for exploring the biological functions of GSH and potentially serve as a therapeutic technology for GSH-related tumours.

CRediT authorship contribution statement

Yu Liu: Software, Investigation, Data curation. **Rui Wang:** Resources, Methodology, Investigation, Data curation. **Yonghai Wang:** Methodology, Investigation, Data curation. **Guiling Zhao:** Software, Project administration, Investigation, Formal analysis. **Kun Dou:** Writing – review & editing, Writing – original draft, Funding acquisition, Data curation, Conceptualization. **Yanlong Xing:** Formal analysis, Data curation. **Fabiao Yu:** Writing – review & editing, Supervision, Conceptualization.

Declaration of Competing Interest

The authors declare that they have no known competing financial interests or personal relationships that could have appeared to influence the work reported in this paper.

Acknowledgments

This work was supported by the Key Research and Development projects in Hainan Province (ZDYF2022SHFZ288); National Natural Science Foundation of China (No. 22204037); Hainan Provincial Natural Science Foundation of China (No. 823QN245); NanHai Rising Star Technology and Innovation Talent project of Hainan Province (NHXXRCXM202319), and The Talent Research Launch Fund of Hainan Medical University (XRC2022003).

Appendix A. Supporting information

Supplementary data associated with this article can be found in the online version at [doi:10.1016/j.snb.2024.137005](https://doi.org/10.1016/j.snb.2024.137005).

Data availability

Data will be made available on request.

References

- [1] Z. Zhang, L. Zhou, N. Xie, E.C. Nice, T. Zhang, Y. Cui, et al., Overcoming cancer therapeutic bottleneck by drug repurposing, *Sig. Transduct. Target. Ther.* 5 (2020) 113.
- [2] E.J. Ge, A.I. Bush, A. Casini, P.A. Cobine, J.R. Cross, G.M. DeNicola, et al., Connecting copper and cancer: from transition metal signalling to metalloplasia, *Nat. Rev. Cancer* 22 (2022) 102–113.
- [3] D.Q. Huang, H.B. El-Serag, R. Loomba, Global epidemiology of NAFLD-related HCC: trends, predictions, risk factors and prevention, *Nat. Rev. Gastro. Hepat.* 18 (2021) 223–238.
- [4] M.M. Kim, A. Parolia, M.P. Dunphy, S. Venneti, Non-invasive metabolic imaging of brain tumours in the era of precision medicine, *Nat. Rev. Clin. Oncol.* 13 (2016) 725–739.
- [5] M. van Essen, A. Sundin, E.P. Krenning, D.J. Kwekkeboom, Neuroendocrine tumours: the role of imaging for diagnosis and therapy, *Nat. Rev. Endocrinol.* 10 (2014) 102–114.
- [6] E.G.E. de Vries, L. Kist de Ruijter, M.N. Lub-de Hooge, R.A. Dierckx, S.G. Elias, S. F. Oosting, Integrating molecular nuclear imaging in clinical research to improve anticancer therapy, *Nat. Rev. Clin. Oncol.* 16 (2019) 241–255.
- [7] M.D. Farwell, D.A. Pryma, D.A. Mankoff, PET/CT imaging in cancer: current applications and future directions, *Cancer* 120 (2014) 3433–3445.
- [8] J.R. Fink, M. Muzi, M. Peck, K.A. Krohn, Multimodality brain tumor imaging: MR imaging, PET, and PET/MR imaging, *J. Nucl. Med.* 56 (2015) 1554–1561.
- [9] K. Wang, Y. Du, Z. Zhang, K. He, Z. Cheng, L. Yin, et al., Fluorescence image-guided tumour surgery, *Nat. Rev. Bioeng.* 1 (2023) 161–179.
- [10] E.L. Schmidt, Z. Ou, E. Ximenes, H. Cui, C.H. Keck, D. Jaque, et al., Near-infrared II fluorescence imaging, *Nat. Rev. Methods Primers* 4 (2024) 23.
- [11] P.P. Ghoroghchian, M.J. Therien, D.A. Hammer, In vivo fluorescence imaging: a personal perspective, *Wires Nanomed. Nanobiotechnol.* 1 (2009) 156–167.
- [12] M. Koch, P. Symvoulidis, V. Ntziachristos, Tackling standardization in fluorescence molecular imaging, *Nat. Photonics* 12 (2018) 505–515.
- [13] G. Hong, A.L. Antaris, H. Dai, Near-infrared fluorophores for biomedical imaging, *Nat. Biomed. Eng.* 1 (2017) 0010.
- [14] A.L. Antaris, H. Chen, K. Cheng, Y. Sun, G. Hong, C. Qu, et al., A small-molecule dye for NIR-II imaging, *Nat. Mater.* 15 (2016) 235–242.
- [15] H. Li, Y. Kim, H. Jung, J.Y. Hyun, I. Shin, Near-infrared (NIR) fluorescence-emitting small organic molecules for cancer imaging and therapy, *Chem. Soc. Rev.* 51 (2022) 8957–9008.
- [16] B. Li, M. Zhao, J. Lin, P. Huang, X. Chen, Management of fluorescent organic/inorganic nanohybrids for biomedical applications in the NIR-II region, *Chem. Soc. Rev.* 51 (2022) 7692–7714.
- [17] H. Wan, J. Yue, S. Zhu, T. Uno, X. Zhang, Q. Yang, et al., A bright organic NIR-II nanofluorophore for three-dimensional imaging into biological tissues, *Nat. Commun.* 9 (2018) 1171.
- [18] J. Mu, M. Xiao, Y. Shi, X. Geng, H. Li, Y. Yin, et al., The chemistry of organic contrast agents in the NIR-II window, *Angew. Chem. Int. Ed.* 61 (2022) e202114722.
- [19] L. van Manen, H.J. Handgraaf, M. Diana, J. Dijkstra, T. Ishizawa, A.L. Vahreijer, et al., A practical guide for the use of indocyanine green and methylene blue in fluorescence-guided abdominal surgery, *J. Surg. Oncol.* 118 (2018) 283–300.
- [20] K. He, C. Chi, D. Kou, W. Huang, J. Wu, Y. Wang, et al., Comparison between the indocyanine green fluorescence and blue dye methods for sentinel lymph node biopsy using novel fluorescence image-guided resection equipment in different types of hospitals, *Transl. Res.* 178 (2016) 74–80.
- [21] X. Zhao, C.X. Yang, L.G. Chen, X.P. Yan, Dual-stimuli responsive and reversibly activatable theranostic nanoprobe for precision tumor-targeting and fluorescence-guided photothermal therapy, *Nat. Commun.* 8 (2017) 14998.
- [22] Y. Shen, X. Le, Y. Wu, T. Chen, Stimulus-responsive polymer materials toward multi-mode and multi-level information anti-counterfeiting: recent advances and future challenges, *Chem. Soc. Rev.* (2024).
- [23] Y. Wang, Y. Hu, D. Ye, Activatable multimodal probes for in vivo imaging and theranostics, *Angew. Chem. Int. Ed.* 134 (2022) e202209512.
- [24] R. He, D. Tang, N. Xu, H. Liu, K. Dou, X. Zhou, et al., Evaluation of erastin synergized cisplatin anti-nasopharyngeal carcinoma effect with a glutathione-activated near-infrared fluorescent probe, *Chin. Chem. Lett.* 35 (2024) 108658.
- [25] H. Li, D. Kim, Q. Yao, H. Ge, J. Chung, J. Fan, et al., Activity-based NIR enzyme fluorescent probes for the diagnosis of tumors and image-guided surgery, *Angew. Chem. Int. Ed.* 133 (2021) 17408–17429.
- [26] S. Prasad, S.C. Gupta, A.K. Tyagi, Reactive oxygen species (ROS) and cancer: Role of antioxidative nutraceuticals, *Cancer Lett.* 387 (2017) 95–105.
- [27] H. Sies, D.P. Jones, Reactive oxygen species (ROS) as pleiotropic physiological signalling agents, *Nat. Rev. Mol. Cell Bio.* 21 (2020) 363–383.
- [28] L. Wu, X. Qu, Cancer biomarker detection: recent achievements and challenges, *Chem. Soc. Rev.* 44 (2015) 2963–2997.
- [29] L.B. Sullivan, D.Y. Gui, M.G.V. Heiden, Altered metabolite levels in cancer: implications for tumour biology and cancer therapy, *Nat. Rev. Cancer* 16 (2016) 680–693.
- [30] C. Gorrini, I.S. Harris, T.W. Mak, Modulation of oxidative stress as an anticancer strategy, *Nat. Rev. Drug. Discov.* 12 (2013) 931–947.
- [31] X. Cheng, H.D. Xu, H.H. Ran, G. Liang, F.G. Wu, Glutathione-depleting nanomedicines for synergistic cancer therapy, *ACS Nano* 15 (2021) 8039–8068.
- [32] Y. Xiong, C. Xiao, Z. Li, X. Yang, Engineering nanomedicine for glutathione depletion-augmented cancer therapy, *Chem. Soc. Rev.* 50 (2021) 6013–6041.

- [33] K. Umezawa, M. Yoshida, M. Kamiya, T. Yamasoba, Y. Urano, Rational design of reversible fluorescent probes for live-cell imaging and quantification of fast glutathione dynamics, *Nat. Chem.* 9 (2017) 279–286.
- [34] Y.L. Liu, S.-Y. Yu, R. An, Y. Miao, D. Jiang, D. Ye, et al., A fast and reversible responsive bionic transmembrane nanochannel for dynamic single-cell quantification of glutathione, *ACS Nano* 17 (2023) 17468–17475.
- [35] X. Jiang, J. Chen, A. Bajić, C. Zhang, X. Song, S.L. Carroll, et al., Quantitative real-time imaging of glutathione, *Nat. Commun.* 8 (2017) 16087.
- [36] Y. Huang, S. Wu, L. Zhang, Q. Deng, J. Ren, X. Qu, A metabolic multistage glutathione depletion used for tumor-specific chemodynamic therapy, *ACS Nano* 16 (2022) 4228–4238.
- [37] M.Y. Lucero, J. Chan, Photoacoustic imaging of elevated glutathione in models of lung cancer for companion diagnostic applications, *Nat. Chem.* 13 (2021) 1248–1256.
- [38] Y. Pan, S. Lei, J. Zhang, J. Qu, P. Huang, J. Lin, Activatable NIR-II fluorescence probe for highly sensitive and selective visualization of glutathione in vivo, *Anal. Chem.* 93 (2021) 17103–17109.
- [39] Y. Yue, T. Zhao, Z. Xu, W. Chi, X. Chai, J. Ai, et al., Enlarging the Stokes shift by weakening the π -conjugation of cyanines for high signal-to-noise ratiometric imaging, *Adv. Sci.* 10 (2023) 2205080.
- [40] A. Refaat, M.L. Yap, G. Pietersz, A.P.G. Walsh, J. Zeller, B. del Rosal, et al., In vivo fluorescence imaging: success in preclinical imaging paves the way for clinical applications, *J. Nanobiotech.* 20 (2022) 450.
- [41] Q. Ding, X. Wang, Y. Luo, X. Leng, X. Li, M. Gu, et al., Mitochondria-targeted fluorophore: state of the art and future trends, *Coord. Chem. Rev.* 508 (2024) 215772.

Yu Fabiao, PhD, researcher, doctoral supervisor, graduated from Dalian University of Technology / Dalian Institute of Chemical Physics, Chinese Academy of Sciences in 2013. He is the head of Functional Materials and Molecular Imaging Technology Innovation Team of Hainan Medical College (the first batch of Double Hundred Teams of Hainan Province), the Hundred Talents Programme of Hainan Province, the leading high-level talents of Hainan Province, the second level candidate of '515 Talents Project' of Hainan Province, the reserve candidate of Hainan Provincial Party Committee's contact service key experts, the member of Youth Innovation Promotion Association of Chinese Academy of Sciences, the executive director of Hainan Biomedical Engineering Society, the member of the Degree Committee of Hainan Province, the member of Graduate Teaching Committee of Professional Degrees, and the member of Graduate Discipline Evaluation Group of Hainan Degree Committee. He is also a member of Hainan Provincial Academic Degree Committee, the Professional Degree Graduate Teaching Committee, and Hainan Provincial Academic Degree Committee Graduate Discipline Review Group. He is the director of the Key Laboratory of Functional Materials and Molecular Imaging Technology of Hainan Medical College, the director of the Key Laboratory of Trauma and Disaster Rescue Research of Hainan Province, and the director of the Engineering Research Centre of Biomaterials and Medical Devices of Hainan Province.